Diamond & Related Materials 31 (2013) 58–64

Contents lists available at SciVerse ScienceDirect

Diamond & Related Materials

journal homepage: www.elsevier.com/locate/diamond

Corrosion, wear and wear–corrosion behavior of graphite-like *a*-C:H films deposited on bare and nitrided titanium alloy

T.M. Manhabosco [a,*], A.P.M. Barboza [b], R.J.C. Batista [a], B.R.A. Neves [b], I.L. Müller [c]

[a] Physics Department, Federal University of Ouro Preto, Campus Universitário Morro do Cruzeiro ICEB/DEFIS, 35400-000, Ouro Preto, Minas Gerais, Brazil
[b] Physics Department, Federal University of Minas Gerais, Av. Antonio Carlos 6627, 31270-901, Belo Horizonte, Minas Gerais, Brazil
[c] Metallurgy Department, Laboratory of Corrosion Research, Federal University of Rio Grande do Sul, Av. Bento Gonçalves 9500/75/232, 91501-970, Porto Alegre, Rio Grande do Sul, Brazil

ARTICLE INFO

Article history:
Received 1 April 2012
Received in revised form 28 September 2012
Accepted 7 November 2012
Available online 15 November 2012

Keywords:
Diamond-like carbon
Tribology
Corrosion
Scanning probe techniques

ABSTRACT

This work presents a comparative wear, corrosion and wear–corrosion (the last one in a simulated physiological solution) study of graphite-like *a*-C:H (GLCH) films deposited on bare and nitrided Ti6Al4V alloy. Films, deposited by r.f. PACVD, presented low porosity and promoted high corrosion resistance. The friction coefficient of the films was very low with appreciable wear resistance at room conditions. However, due to the simultaneous action of both load and the corrosive environment in wear–corrosion tests a marked reduction in the coating lifetime was observed. Unexpectedly, films deposited on the nitrided alloy presented a lifetime at least ten times shorter than that of films on bare alloy. We explain such a result in terms of film/substrate interaction. The weak GLCH/nitrided alloy interaction facilitates fluid penetration between the film and the substrate which leads to a fast film delamination. Such an interpretation is supported by force curve measurements, which show that the interaction between GLCH and nitrided alloy is four times weaker than that between GLCH and bare alloy.

1. Introduction

Among metallic materials, titanium and its alloys have been most commonly chosen for use in implants. This choice is motivated by titanium appropriate properties such as low density, high strength to weight ratio, good corrosion resistance, and above all, biocompatibility which is conferred by the thin and compact oxide (TiO_2) spontaneously formed at its surface in the presence of oxygen [1–3]. However, in some applications (in ankle and hip joints, for instance) superior mechanical wear and, mainly, wear–corrosion resistance are required, but not provided by those metals [4,5]. To extend the use of titanium to situations where superior resistance is required, researchers have been working to improve the surface properties of titanium and its alloys through mechanical, chemical, thermo-chemical processes and/or coating deposition [6–10]. It is worth mentioning the work of Kumar et al. [8] who studied the fretting-corrosion behavior of untreated, anodized and thermally oxidized pure titanium in Ringer's solution and observed an increase in the fretting-corrosion resistance after surface treatment. The thermally oxidized samples presented better fretting-corrosion resistance.

Regarding high performance coatings, diamond-like carbon (DLC) films have been pointed out as good candidates for coat implants such as hip and ankle joints besides heart valves and stents [11–13]. In fact, DLC films present exceptional properties such as wear resistance, high hardness, low friction coefficient, corrosion resistance, good bio- and hemocompatibilities, high thermal conductivity, optical transparence to infrared and chemical inertness [11–16], which support their use in a wide range of applications. DLC is a relatively new class of amorphous carbon materials with a significant content of C – C sp^3 bonds, which confers them some of the properties previously cited. Moreover, DLC films may contain other elements such as hydrogen, nitrogen and silicon that can alter their structure and properties [16–18]. The hydrogenated amorphous carbons are classified into four types: polymer-like a-C:H (PLCH), films with 40–60 at.% of H content; diamond-like a-C:H (DLCH), films with 20–40 at.% of H content; hydrogenated tetrahedral amorphous carbon films (ta-C:H); and graphite-like a-C:H (GLCH) with low H content (less than 20 at.%).

Besides the appropriate properties of the films, their adhesion to the substrate is mandatory for a biomaterial to be implanted inside a living body. One problem regarding DLC films on titanium and its alloys is the failure and detachment of the coating. The failure of the coating may be due to the plastic deformation of the substrate, the cracking of the coating and/or the failure of the interface since there is a mismatch in the mechanical and chemical properties of those two materials (i.e., the hard and brittle coating is not capable of withstanding plastic deformation as well as the soft substrate which results in cracks and delamination of the film). Interlayers and surface treatments have been used to overcome this problem and improve the load-bearing capacity as they provide a gradual change in the hardness and better tension distribution from the coating to the substrate [19–21]. Such treatments and interlayers indeed improve the films resistance to wear or corrosion in situations where load and corrosive environment are not acting together. However, in some applications, like ankle and hip joints, load and a

* Corresponding author at: Campus Universitário Morro do Cruzeiro ICEB/DEFIS, Ouro Preto, Minas Gerais, 35400-000, Brazil. Tel.: +55 31 35591675; fax: +55 31 35591667.
E-mail address: taisemanhabosco@gmail.com (T.M. Manhabosco).

0925-9635/$ – see front matter © 2012 Elsevier B.V. All rights reserved.
http://dx.doi.org/10.1016/j.diamond.2012.11.005

corrosive environment must be taking into account. Unfortunately, in wear–corrosion solicitations a catastrophic failure of the DLC films has been recently observed [22] showing that DLC coatings cannot safely be used yet in situations in which load and corrosive environment are acting together. To extend the use of DLC coatings to such situations, it is mandatory to understand the features related to the catastrophic failure mechanism.

In the present work we investigate the changes in the mechanical and electrochemical behavior of bare and nitrided Ti6Al4V alloy surfaces due to the GLCH coating deposited by r.f. PACVD. We observe a catastrophic failure of GLCH films on both substrates in wear–corrosion tests. In spite of the hardness gradient and better physical anchorage provided by the roughness of the nitrided substrate, the coating deposited on it fails much earlier than that deposited on bare alloy.

2. Experimental details

2.1. Materials, surface treatment and coating deposition

Ti6Al4V alloy (grade 5) disc samples with 38 mm in diameter and mean thickness of 17 mm were obtained from a bar. Samples were ground with SiC emery paper to 800 grit and polished with colloidal silica. After polishing, the samples were ultrasonically cleaned in acetone for 10 min followed by rinsing in methanol and deionized water. After preparation, the surface roughness (R_a) of the samples was about 25 nm.

Some samples were nitrided in a gas mixture of 10% Ar, 50% H_2 and 40% N_2 at 300 Pa for 10 h. The temperature of the process (1073 K) was chosen below the transition temperature of the alloy (1228 K). The nitrided layer microstructure was analyzed by X-ray diffraction (X Philips — X'Pert MRD) with Cu Kα radiation ($\lambda = 1.5406$ Å).

The coatings were commercially deposited on the Ti6Al4V polished samples and on the nitrided samples (not polished after nitriding process) using r.f. (13.56 MHz) PACVD technique. The samples were placed at the top of the chamber to avoid dust particles. Prior to deposition the reaction chamber was evacuated to a base pressure of ca. 1.5 Pa and samples were cleaned by sputtering with argon (Ar) for 20 min. The deposition was performed at 1.5 Pa with acetylene (C_2H_2) flowing at a rate of 50 sccm for 2 h. The negative self-bias voltage of the r.f. powered electrodes was 1000 V. Thirty bare and thirty nitrided Ti6Al4V samples were single side coated with 4 μm thick films.

2.2. Surface and coating characterizations

The nitrided samples were characterized by scanning electron microscopy (SEM) and X-ray diffraction as previously published [23].

The surface morphology of the coatings deposited on bare and nitrided samples was acquired by atomic force microscopy (AFM — Shimadzu model SPM-9500J3) in the contact mode and the surface roughness was estimated from AFM images. The coatings were analyzed by Raman spectroscopy performed with a NTEGRA Spectra Nanofinder (NT-MDT) operating at 514.5 nm excitation. The coating hardness was acquired from nanoindentation tests using a CETR nanohardness tester. The maximum load in each indentation was 100 mN with no penetration depth higher than 20% of the film thickness. A Vickers indenter and the Oliver and Pharr [24] method were used to determine hardness.

A Nanoscope IV MultiMode SPM, from Veeco Instruments, was employed for force spectroscopy analysis of bare and nitride samples. SPM measurements were carried out in air, or under dry nitrogen atmospheres, with the help of homemade environmental control chambers. Heating experiments were carried out with a commercial hot stage AFM setup (Veeco Instruments MultiMode SPM with High Temperature Heater accessory). The used silicon cantilevers were covered with a thin doped-diamond film, from NT-MDT, with $k \sim 2.5$–10 N/m, $R \sim 30$–50 nm and $\omega_0 \sim 115$ to 190 kHz. More accurate estimations of k and R were carried out by the use of the Sader's method [25] and by imaging reference samples, respectively. During the heating process, most of the water layer is removed. This layer is responsible for the capillary forces when the tip comes into contact with the sample surface and a water meniscus is formed. Therefore, using the hot stage, the adhesion force between the diamond tip and the sample surface can be measured with reduced influence of the water layer.

2.3. Corrosion tests

The corrosion behavior of the samples was evaluated by means of potentiodynamic polarization curves in a simulated body fluid environment (phosphate buffered saline solution (PBS)) at a scan rate of 0.167 mV/s using an EG&G 273A potentiostat. The PBS solution used was composed of 8 g/l NaCl; 0.2 g/l KCl; 0.594 g/l Na_2HPO_4 and 0.2 g/l KH_2PO_4, pH = 7.1. The tests were performed in a three-electrode cell with the temperature controlled at 37 °C (±1 °C) by a thermostatic bath. A saturated calomel electrode (SCE) was used as reference electrode and platinum wire as counter electrode. The exposed area of the samples (3.14 cm^2) was determined by a Teflon o-ring. Before the beginning of the corrosion tests the system was maintained 1 h in the solution in order to stabilize the open circuit potential (OCP).

The protective efficiency of the coatings was determined from the polarization curves by the empirical equation [26]:

$$P_i = 100\left(1 - i_{corr}/i^{\circ}_{corr}\right) \quad (1)$$

where i_{corr} and i°_{corr} are the corrosion current densities in the presence and absence of the coating.

The total coating porosity was estimated from electrochemical measurements using the following equation [27]:

$$P = \left(R_{pm(substrate)}/R_{p\ (coating-substrate)}\right) x 10^{-\left|\Delta E_{corr}/\beta_a\right|} \quad (2)$$

where R_{pm} the polarization resistance of the substrate, R_p the measured polarization, ΔE_{corr} is the potential difference between the free corrosion potentials of the coated alloy and the bare substrate and β_a, the anodic Tafel slope for the substrate.

2.4. Wear tests

The tribological behavior of the films at room conditions (relative humidity about 25% and 20 °C) was evaluated by wear tests carried out in a reciprocating pin-on-plate tribometer controlled by a computer. The tests were performed by applying a normal load of 16 N, sliding velocity of 32 mm/s and 8 mm wear track length. Tests were performed for 2 h or until coating failure. The counter body used was an alumina ball (∅ 5 mm, Saphirwerk). At the end of each wear test, the wear track was analyzed by optical and SEM microcopy. The wear track profile was recorded by a profilometer (MicroGlider, Fries Research & Technology) and the wear volume was integrated from the wear track profile.

2.5. Wear–corrosion tests

To perform the wear–corrosion tests the electrochemical cell used in the corrosion tests was coupled to the tribometer. The counter and reference electrodes were the same as used for the other electrochemical tests with the electrodes distant no more than 1 cm from the wear track. The tests were carried out in PBS solution at open potential circuit (OCP) and at an anodic potential of 0.4 V_{SCE} with a temperature of 37 °C (±1 °C). Before the beginning of the wear–corrosion tests the system was maintained 1 h in the solution in order to stabilize the open circuit potential (OCP). The wear parameters were the same as those used in single wear tests, i.e., normal load of 16 N, sliding velocity of 32 mm/s and wear track length of 8 mm. Tests were performed for 2 h or until the coating failed. The tests performed until the coating failed were repeated more than eight times.

At the end of each wear–corrosion test, the wear track profile was recorded by a profilometer and the wear track volume was calculated by integrating the wear track profile. The wear track was also analyzed by optical and SEM microcopy.

3. Results and discussion

3.1. Coatings

Atomic force microscopy images of the coatings deposited on bare and nitrided alloy are shown in Fig. 1. Films deposited on bare alloy are composed of small compact grains homogeneously distributed on the surface with a mean roughness (R_a) of about 7.9 nm calculated from 9×9 μm images. Films deposited on nitrided samples show large grains composed of agglomerated small grains with a roughness (R_a) of about 61.2 nm obtained from 9×9 μm images. The difference in the coating morphology can be ascribed to the substrate chemical composition and morphology, since the alloy was exposed to both the sputtering process, for oxide removal, and nitriding process [28]. Also, secondary electron emission from the two substrates (bare and nitride samples) increases differently the plasma intensity that results in different coating morphology and properties [29]. It should be pointed out that the nitriding process was responsible for the formation of the Ti_2N phase (tetragonal) and the TiN phase (cubic face centered) and also for increasing the surface roughness of Ti6Al4V samples from (R_a) of 25 nm to about (R_a) 150 nm [23].

The coatings deposited on both bare and nitrided samples were characterized by Raman spectroscopy as shown in Fig. 2. The spectral shape was fitted with Gaussians that reveals the common features of DLC films, the so-called D and G peaks. The D peak lies at approximately 1385 cm^{-1} while the G peak lies at around 1569 cm^{-1}. Ferrari et al. [30] have shown that Raman spectroscopy is a powerful technique to characterize DLC films. According to Fig. 3 of their manuscript, the position of G peak of our films corresponds to an sp^3 content of about 33%. The amount of H in the film can be estimated from the photoluminescence background slope as shown by Casiraghi et al. [18]. Using the equation below (Eq. (1) of Ref. [18]), we obtained a hydrogen content of about 16%.

$$H[\text{at. }\%] = 21.7 + 16.6\log\{m/I(G)[\mu m]\} \quad (3)$$

where m is the slope of the spectra measured between 1050 and 1800 cm^{-1} and I(G) is the height of the G peak.

Indeed, the spectrum shown in Fig. 4 is very similar to those of Casiraghi et al. [18] for the same hydrogen content. The amount of hydrogen combined with the sp^3 content allows us to determine the sp^2 content from the ternary diagram presented by Casiraghi et al. [31]. Hydrogenated amorphous carbon with 33% of sp^3 bonds and a hydrogen content of 16% presents a sp^2 content of 51% resulting in a sp^3/sp^2 ratio of 0.65.

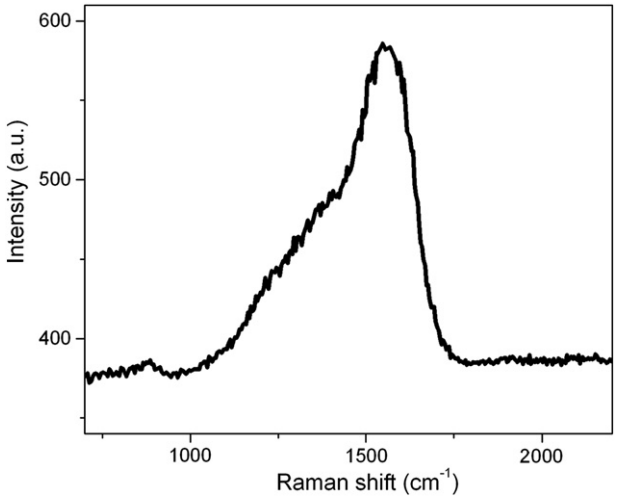

Fig. 2. Raman spectra of the coatings deposited r.f. (13.56 MHz) PACVD at 514.5 nm excitation.

According to Casiraghi et al. [31], films with low H content, lower than 20%, present a high sp^2 content and clustering with a band gap lower than 1 eV. Casiraghi et al. [18,31] used the term graphite-like hydrogenated amorphous carbons (GLCH) to denominate this type of DLC films with low H content. The I_D/I_G ratio, a qualitative indicator of the nature of the bond and degree of graphitization, was calculated as being 0.60

The nanohardness measurements of the films result in values of 16.87±0.54 GPa. The literature presents a wide range of values for DLC film nanohardness that is mainly related to the amount of hydrogen incorporated into the film, to the I_D/I_G ratio and sp^3 content [32–34].

3.2. Corrosion results

Fig. 3 presents the potentiodynamic polarization curves in PBS solution for the bare alloy, the nitrided alloy and the GLCH coatings deposited on both bare and nitrided alloy. The bare alloy presents a passive behavior in the simulated body fluid environment with anodic current densities of about 8×10^{-7} A/cm^2 in a wide range of anodic potentials. The electrochemical behavior after nitriding indicates that

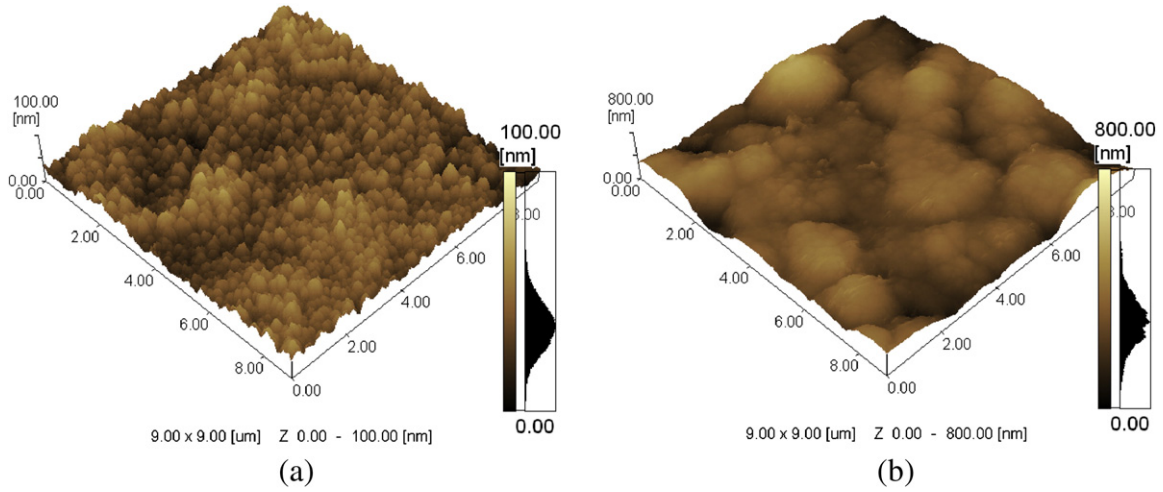

Fig. 1. AFM images of DLC films deposited on bare (a) and nitrided (b) alloy.

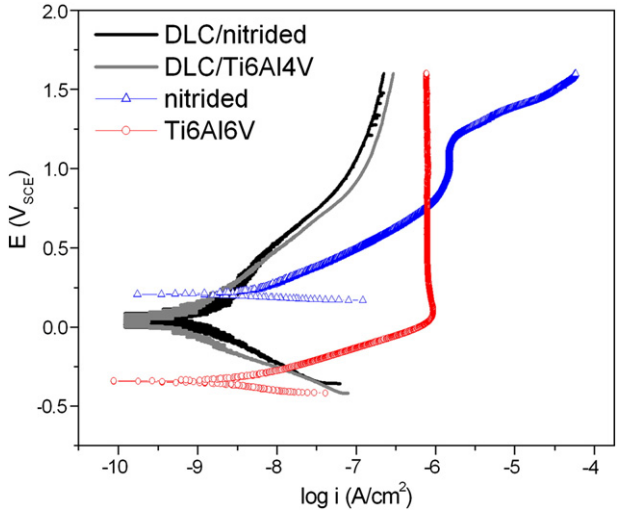

Fig. 3. Potentiodynamic polarization curves in PBS solution for bare alloy, nitrided alloy and DLC film deposited on both bare and nitrided alloy. Sweep rate: 0.167 mV/s.

the alloy becomes nobler and with lower anodic current densities until 0.75 V_{SCE}, indicating an increase in the corrosion resistance. At higher potentials an anodic peak is found that, according to the Pourbaix diagram proposed by Heide and Schultze [35], may correspond to the oxidation of TiN to TiO_2 as previously published [23].

GLCH films deposited on both bare and nitrided samples present similar behavior with lower current densities indicating superior corrosion protection. The protective efficiency and porosity of the films deposited onto bare alloy were calculated as being about 97% and 0.01, and for GLCH films deposited on nitride samples as being around 95% and 0.02. Statistically there is no significant difference in the values and comparing the polarization curves in the PBS solution, for GLCH deposited on both substrates, they present no important differences. Only at higher overpotentials the GLCH deposited on nitrided alloy presents some breaks that could be associated with the oxidation of TiN to TiO_2.

3.3. Wear results

From the wear tests performed at room conditions a friction coefficient of about 0.43 and 0.38 was found for nitrided and bare alloy, respectively. Samples coated with GLCH presented an expressive reduction in the friction coefficient; values of about 0.04 were observed, in agreement with data reported in the literature [37–41]. As expected for a hard material with a low friction coefficient the wear track volume was very low, 6.5×10^{-13} m^3 for films deposited on nitrided alloy and 4.0×10^{-13} m^3 for films on bare alloy. Such values correspond to wear rates of 1.76×10^{-7} mm^3/Nm and 1.8×10^{-7} mm^3/Nm, respectively. Such a difference is probably related to the roughness of GLCH coatings deposited on nitrided alloy since at the beginning of the wear test the load concentrates at the top of the asperities (the shear stress at the tops of the asperities is higher due to their small area). Bare samples tested with the same parameters showed a wear track volume some 3700 times larger, which indicates that GLCH is an excellent coating to improve the wear resistance of titanium alloy in room conditions.

Several tests were carried out until the coating failed. GLCH films deposited on bare alloy resisted from 4.1 up to 4.6 km wear distance, while films deposited on nitrided alloy resisted from 4.2 up to 5.4 km until failure. This slight increase in the mean lifetime could be related to the hardness gradient of GLCH films deposited on nitrided samples (which present a diffusion zone along 30 μm from the top surface) that avoid the eggs shell effect and/or to the better physical anchorage provided by the roughness (see Section 3.1).

3.4. Wear- corrosion results

The wear–corrosion behavior of the films at OCP conditions was monitored for 2 h as shown in Fig. 4. The vertical line indicates the beginning of wear.

It can be observed after beginning of wear that potential of GLCH coated bare alloy decreases slowly until the end of the test. Such a decreasing behavior can be related to the combined action of the normal wear force and corrosive environment through film pores and/or microcracks formed during the test.

GLCH films deposited on bare alloy suffer low wear after the two hour test, as can be seen in Fig. 5. The total wear volume calculated in this sample was about 5×10^{-14} m^3, which corresponds to a wear rate of 1.37×10^{-8} mm^3/Nm. After the test the alumina ball was analyzed in SEM and optical microscope and no transferred layer or damage could be observed.

Films deposited on nitrided alloy, on the other hand, suffered a catastrophic failure 16 min after wear began, that represents a wear distance of only 0.03 km in wear–corrosion tests. After failure the potential abruptly changes to values representative of bare alloy indicating the complete removal of both GLCH film and nitrided layer. According to the GLCH/nitrided wear profile (Fig. 5) a deep wear track of 1×10^{-4} m, a value higher than the thickness of the GLCH coating plus the compound layer plus diffusion zone, confirms the attainment of the bare alloy. The total wear volume was around 4.7×10^{-4} m^3 (wear rate of 127.5 mm^3/Nm), 10^{10} times higher than in the case of GLCH deposited on bare alloy. Fig. 6 shows the severe damages on the sample and on the counter-body after wear–corrosion test. It can be observed that the counter-body was severely damaged and presents a transferred layer. The morphology of the wear track clearly indicates the occurrence of film delamination on borders, asperity deformation and ploughing.

Fig. 7 presents the i_{anod} versus time behavior obtained from wear–corrosion tests at an anodic potential of 0.4 V_{SCE} and also the corrosion behavior of the bare alloy at 0.4 V_{SCE} without wear for comparison. The GLCH coatings deposited on nitrided alloy also fail, in agreement with results obtained in wear–corrosion tests at OCP conditions. The lifetime of the films was between 0.02 and 0.03 km, and after coating failure the corrosion current density fast reaches that of bare alloy, around 2×10^{-4} A/cm^2. The current density oscillations on bare alloy are due to rapid repassivation after mechanical wear, i.e. depassivation/repassivation events [23,36].

In a previous work [23] it was shown that the nitriding process increases the wear–corrosion resistance of Ti6Al4V alloy; thus one

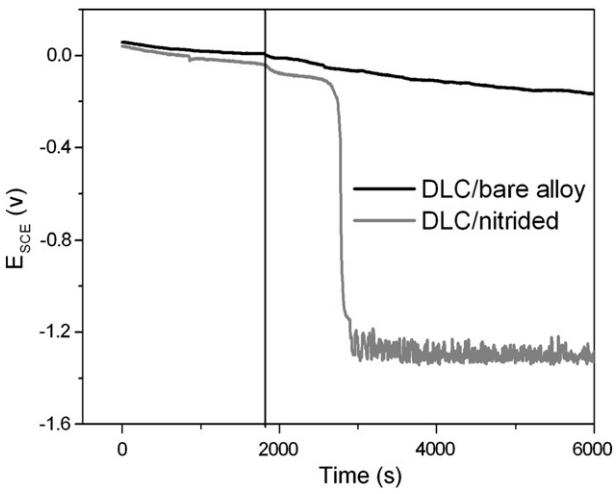

Fig. 4. Evolution of the OCP of DLC films deposited on bare and nitrided alloy. The vertical line indicates the beginning of wear at a normal force of 16 N and sliding velocity of 32 mm/s.

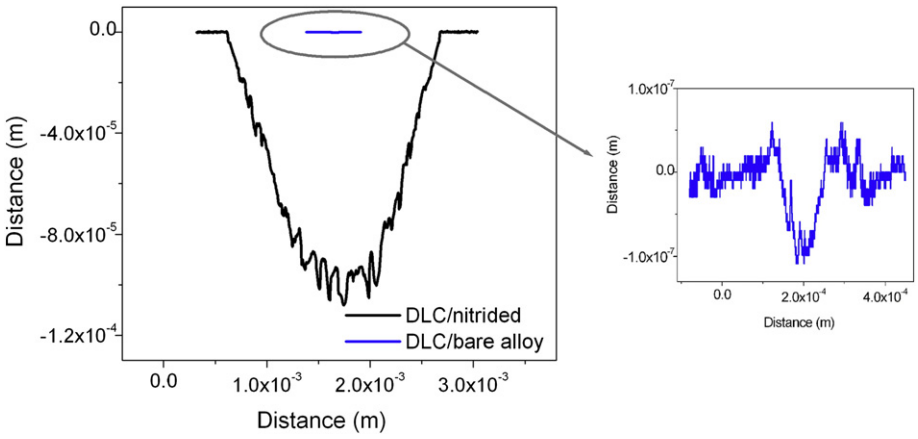

Fig. 5. Wear track profile of DLC deposited on bare and nitrided samples (a) after 2 h of wear–corrosion test at OCP and wear at a normal load of 16 N and sliding velocity of 32 mm/s. The wear track on bare alloy is amplified for a better view of its profile.

could expect that the nitrided layer should provide additional wear–corrosion protection after the GLCH failure. However, the injection of hard and chemically stable GLCH particles, which act as a hard third body, combined with the high normal load cause severe damage to the material (including the nitrided layer) and to the counter-body. The worn material and counter-body also inject new particles into the contact region and other wear mechanisms such as fatigue and adhesive wear take place simultaneously besides corrosion and abrasive wear.

GLCH films deposited on bare alloy develop an anodic current density about 1.6×10^{-8} A/cm^2 during 2 h of test, indicating superior wear–corrosion protection under the tested conditions. However, films deposited onto bare alloy also fail and the distance to failure varied from 0.37 up to 2 km. Since all tested GLCH coatings present pores that allow the diffusion of ions and water penetration into them, the failure could be associated to the loss of adhesion between the GLCH/metal and to GLCH/metal interface degradation associated to the action of both load and corrosive environment. The film deposited on bare alloy showed a wide range of rubbing distances until failure that can be associated to the probability of occurrence of defects on the wear track or near it (close enough to suffer the adverse effect of both load and corrosive environment). Films free of pores or with no through-film defects, that do not allow water and ions to reach the film/substrate interface, can be good candidates to increase the tribocorrosion resistance. Park et al. [42] tested DLC coatings deposited on Ti6Al4V using a ball-on-disk type wear rig, some in aqueous environment (deionized water) and others in ambient air of relative humidity about 25%. Films tested in aqueous environment presented delamination, which can be closely related to the penetration of water via through-film defects that cause degradation of the interfacial strength. Authors suggest that the lifetime

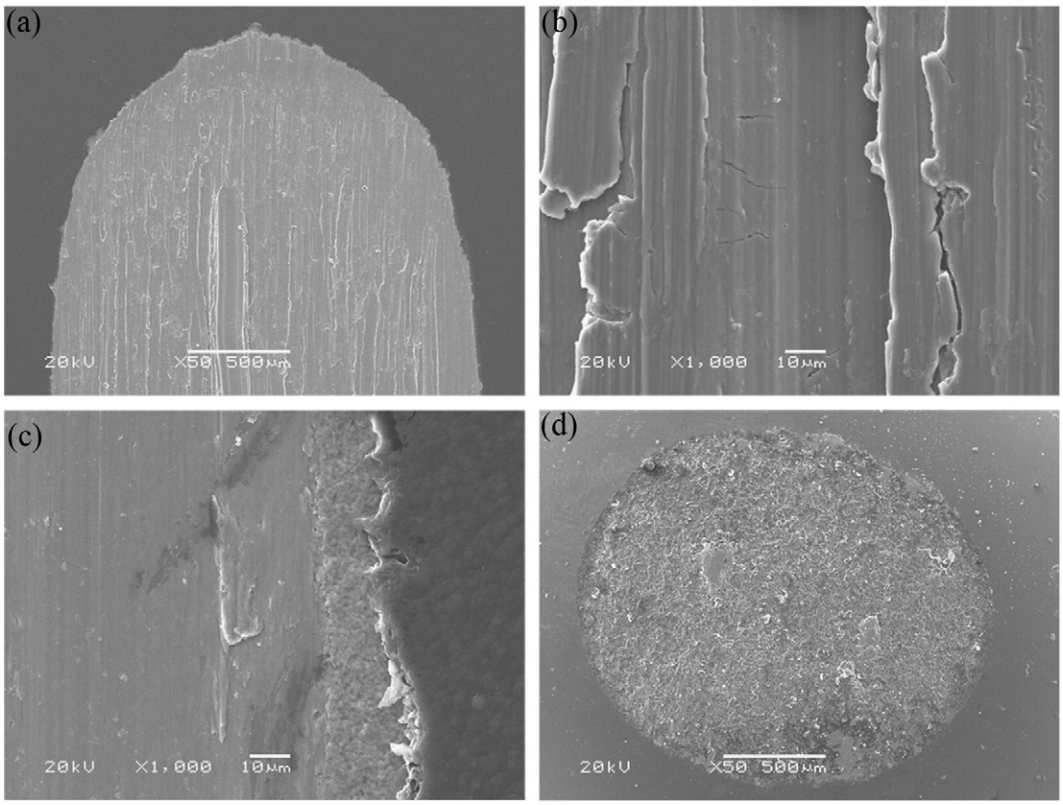

Fig. 6. SEM images of the wear track after 2 h of wear–corrosion test at OCP for nitrided alloy covered by DLC. In (a) is presented the end of the wear track, (b) shows the center of the wear track and (c) presents the wear track edge. The damage to the alumina counter-body is showed in (d).

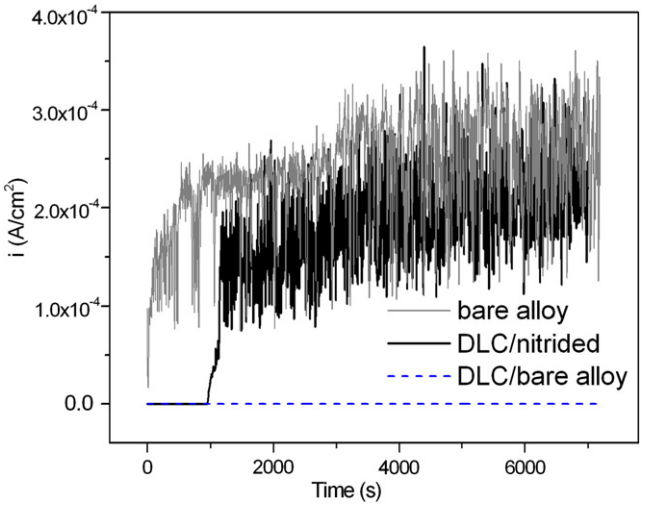

Fig. 7. Evolution of the anodic current density with time in wear–corrosion tests at 0.4 V_{SCE}, wear at a normal force of 16 N and sliding velocity of 32 mm/s.

of the coating can be increased by eliminating the through-film defects and prove that multi-step coating was a good alternative to reduce through-film defects.

In wear tests, films deposited on nitrided alloy tested at room conditions presented a longer lifetime than films deposited on bare Ti6Al4V. However, when wear–corrosion tests were performed the lifetime of coatings deposited on nitrided alloy was significantly reduced compared to that deposited onto bare alloy, despite the hardness gradient and higher roughness. The porosity index in GLCH deposited on nitrided samples is a little higher than that of GLCH on bare samples, therefore, the observed reduction in lifetime cannot be associated with the film porosity. One possibility for this occurrence could be poor chemical affinity between the coating and the nitrided layer in comparison to that of GLCH and bare substrate. Water and aggressive ions penetrate into the pores and, due to the poor GLCH/nitride layer chemical affinity, they can more easily penetrate between the GLCH/nitride layer interface leading to its faster degradation. Such an interpretation is supported by AFM force curve measurements acquired with an atomic force microscope between a diamond tip and the substrates (bare Ti6Al4V and nitrided alloy), as presented in Fig. 8.

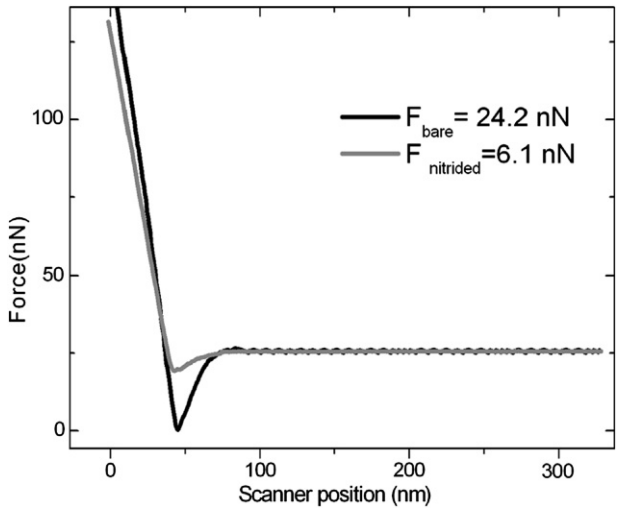

Fig. 8. Experimental force curves for bare (black) and nitrided (gray) alloy using a diamond tip after annealing at 120 °C for 30 min. The smaller adhesion force for the nitrided sample is evident.

It is possible to observe higher adhesion forces between the diamond tip and bare alloy with a pull-off force about 24.2 nN, while the pull-off force for the nitrided alloy was about 6.1 nN. In most cases the adhesion force, defined by intermolecular interactions, is a combination of the electrostatic force, the van der Waals force, the meniscus or capillary force and forces due to chemical bonds [43]. As the meniscus or capillary forces were eliminated by thermal treatment and the pull-off forces are too small to represent chemical bonds, the measured forces are a combination of the remaining forces. The lower adhesion forces observed for the nitrided alloy could be the main cause of premature failure in tribocorrosion tests of the GLCH deposited on nitrided alloy.

4. Conclusions

Diamond-like carbon films with high hardness and low friction coefficient were produced by r.f. PACVD on bare and nitrided Ti6Al4V. Films proven to be effective to improve the wear resistance of bare and nitrided alloy with lifetime extend up to 5.4 km of wear distance in the tested room conditions. Besides, the protective efficiency and porosity of the films indicate a good quality of the films that conferred good corrosion protection on the bare and nitrided alloy.

A catastrophic failure was observed when films were subjected to wear–corrosion conditions. GLCH films deposited on bare alloy presented a reduced lifetime from 0.37 to 2 km while GLCH film deposited on the nitrided sample failed in the first 16 min of the test, which correspond to 0.02–0.03 km lifetime. The catastrophic failure of the films deposited onto both substrates could be related to the water and ions penetration through the pores that could lead to the loss of adhesion between GLCH and substrate and/or to the degradation of GLCH/substrate interface due to the action of both load and corrosive environment.

The premature failure of films deposited on the nitrided alloy could be associated to the weak interaction between GLCH and the nitrided alloy in comparison to that between GLCH and the bare alloy, which was supported by AFM curve forces.

Acknowledgments

The authors wish to acknowledge the financial support of the Brazilian government agencies CNPq, CAPES and FAPEMIG. Authors are grateful to the Fraunhofer Institute (Stuttgart, Germany) for allowing the wear tests and Raman measurements.

References

[1] X. Liu, P.K. Chu, C. Ding, Mater. Sci. Eng. R 47 (2004) 49–121.
[2] M. Niinomi, J. Mech. Behav. Biomed. Mater. 1 (2008) 30–42.
[3] J.L. Katz, in: B.D. Ratner, A.S. Hoffman, F.J. Schoen (Eds.), Biomaterials Science: An Introduction to Materials in Medicine, Academic, Orlando, 1996, pp. 335–346.
[4] F. Contu, B. Elsener, H. Böhni, Electrochim. Acta 50 (2004) 33–41.
[5] T.M. Manhabosco, I.L. Muller, Quim. Nova 32 (2009) 2263–2267.
[6] R. Venugopalan, M.A. George, J.J. Weimer, L.C. Lucas, Biomaterials 20 (1999) 1709–1716.
[7] S. Kumar, T.S.N.S. Narayanan, S.G.S. Raman, S.K. Seshadri, Corros. Sci. 52 (2010) 711–721.
[8] S. Kumar, T.S.N.S. Narayanan, S.G.S. Raman, S.K. Seshadri, Mater. Sci. Eng. C 30 (2010) 921–927.
[9] A.C. Fernandes, F. Vaz, E. Ariza, L.A. Rocha, A.R.L. Ribeiro, A.C. Vieira, J.P. Rivière, L. Pichon, Surf. Coat. Technol. 200 (2006) 6218–6224.
[10] M.K. Lei, Z.H. Dong, Z. Zhang, Y.F. Hu, X.P. Zhu, Surf. Coat. Technol. 201 (2007) 5613–5616.
[11] R. Hauert, Diam. Relat. Mater. 12 (2003) 583–589.
[12] P.D. Maguire, J.A. McLaughlin, T.I.T. Okpalugo, P. Lemoine, P. Papakonstantinou, E.T. McAdams, M. Needham, A.A. Ogwu, M. Ball, G.A. Abbas, Diam. Relat. Mater. 14 (2005) 1277–1288.
[13] G. Thorwarth, C.V. Falub, U. Müller, B. Weisse, C. Voisard, M. Tobler, R. Hauert, Acta Biomater. 6 (2010) 2335–2341.
[14] Y. Wang, L. Wang, S.C. Wang, G. Zhang, R.J.K. Wood, Q. Xue, Tribol. Lett. 40 (2010) 301–310.
[15] C.L. Chen, L.G. Liu, Z.F. Ni, Adv. Mater. Res. 199–200 (2011) 683–688.
[16] R. Hauert, Tribol. Int. 37 (2004) 991–1003.

[17] A.P.M. Barboza, S.S. Carara, R.J.C. Batista, H. Chacham, B.R.A. Neves, Small 8 (2012) 220–224.
[18] C. Casiraghi, F. Piazza, A.C. Ferrari, D. Grambole, J. Robertson, Diam. Relat. Mater. 14 (2005) 1098–1102.
[19] L. Hongxi, J. Yehua, Z. Rong, T. Baoyin, Vacuum 86 (2012) 848–853.
[20] S.B.A. Suilik, M. Ohshima, T. Tetsui, K. Hasezaki, Vacuum 82 (2008) 1325–1331.
[21] J.C. Avelar-Batista, E. Spain, G.G. Fuentes, A. Sola, R. Rodriguez, J. Housden, Surf. Coat. Technol. 201 (2006) 4335–4340.
[22] T.M. Manhabosco, I.L. Müller, Tribol. Lett. 33 (2009) 193–197.
[23] T.M. Manhabosco, S.M. Tamborim, C.B. dos Santos, I.L. Müller, Corros. Sci. 53 (2011) 1786–1793.
[24] W.C. Oliver, G.M. Pharr, J. Mater. Res. 7 (1992) 1564–1583.
[25] J.E. Sader, J.W.M. Chon, P. Mulvaney, Rev. Sci. Instrum. 70 (1999) 3967–3969.
[26] K. Nozawa, K. Aramaki, Corros. Sci. 41 (1999) 57–73.
[27] B. Matthes, E. Broszeit, J. Aromaa, H. Ronkainen, S.-P. Hannula, A. Leyland, A. Matthews, Surf. Coat. Technol. 49 (1991) 489–495.
[28] W. Xu, L.J. Huang, Y.Z. Shih, T. Kim, Y. Hung, G. Li, Thin Solid Films 355–356 (1999) 353–356.
[29] K.S. Mogensen, N.B. Thomsen, S.S. Eskildsen, C. Mathiasen, J. BØtiger, Surf. Coat.Technol. 99 (1998) 140–146.
[30] A.C. Ferrari, B. Kleinsorge, G. Adamopoulos, J. Robertson, W.I. Milne, V. Stolojan, L.M. Brown, A. LiBassi, B.K. Tanner, J. Non-Cryst. Solids 266–269 (2000) 765–768.
[31] C. Casiraghi, A.C. Ferrari, J. Robertson, Phys. Rev. B 72 (2005) 085401–085414.
[32] E. Staryga, G.W. Bak, Diam. Relat. Mater. 14 (2005) 23–34.
[33] G. Messina, A. Paoletti, S. Santangelo, A. Tebano, A. Tucciarone, Microsyst. Technol. 6 (1999) 30–36.
[34] S. Reuter, B. Weßkamp, R. Büscher, B. Barden, F. Löer, V. Buck, Wear 261 (2006) 419–425.
[35] N. Heide, J.W. Schultze, Nucl. Inst. Methods Phys. Res. B 80–81 (1993) 467–471.
[36] J. Komotori, N. Hisamori, Y. Ohmori, Wear 263 (2007) 412–418.
[37] Y. Liu, A. Erdemir, E.I. Meletis, Surf. Coat. Technol. 82 (1996) 48–56.
[38] A. Erdemir, O.L. Eryilmaz, G. Fenske, J. Vac. Sci. Technol. A 18 (2000) 1987–1992.
[39] P. Gupta, E. Meletis, Tribol. Int. 37 (2004) 1031–1038.
[40] C.B. Santos, L. Haubold, H. Holeczek, M. Becker, M. Metzner, Tribol. Lett. 37 (2010) 251–259.
[41] M. Azzi, M. Paquette, J.A. Szpunar, J.E. Klemberg-Sapieha, L. Martinu, Wear 267 (2009) 860–866.
[42] S.J. Park, K.R. Lee, S.-H. Ahn, J.-G. Kim, Diam. Relat. Mater. 17 (2008) 247–251.
[43] H.J. Butt, B. Cappella, M. Kappl, Surf. Sci. Rep. 59 (2005) 1–152.